Carbohydrate Polymers 81 (2010) 925–930

Contents lists available at ScienceDirect

Carbohydrate Polymers

journal homepage: www.elsevier.com/locate/carbpol

Preparation and characterization of cellulose acetate–Fe_2O_3 composite nanofibrous materials

Costas Tsioptsias[a], Kyriaki G. Sakellariou[a], Ioannis Tsivintzelis[a,1], Lambrini Papadopoulou[b], Costas Panayiotou[a,*]

[a] Department of Chemical Engineering, Aristotle University of Thessaloniki, 54124 Thessaloniki, Greece
[b] Department of Geology, Aristotle University of Thessaloniki, 54124 Thessaloniki, Greece

ARTICLE INFO

Article history:
Received 21 August 2009
Received in revised form 25 February 2010
Accepted 7 April 2010
Available online 14 April 2010

Keywords:
Cellulose acetate
Electrospinning
Fe_2O_3
Composite materials
Nanofibers

ABSTRACT

Cellulose acetate (CA) and cellulose acetate–Fe_2O_3 composite nanofibrous materials were successfully prepared via the electrospinning technique. The composite materials were fabricated by the electrospinning of CA solutions with dispersed Fe_2O_3 nanoparticles. A mixture of N,N-dimethylacetamide and acetone was used, in all cases, as the polymer solvent. The Fe_2O_3 nanoparticles were dispersed, in 20% (w/v) CA solution, at concentrations varying between 1.4% and 4.5% (w/v). The influence of Fe_2O_3 concentration on the thermal behavior (glass transition and thermal stability) of the material was examined by means of differential scanning calorimetry (DSC), thermogravimetric analysis (TGA) and infrared spectroscopy (FTIR). Also the influence of Fe_2O_3 concentration on the size and morphology of the fibers was examined by scanning electron microscopy (SEM). For the explanation of the obtained results, viscosity and conductivity measurements were carried out. In general, fairly uniform composite fibrous structures with enhanced properties were prepared, for potential use in separation processes or in biomedical applications.

1. Introduction

Electrospinning is an established technique for the fabrication of micro- and nanofibrous polymer structures. Although the basic principle of the process is quite simple, there are too many parameters involved (e.g. applied voltage, concentration, conductivity and viscosity of the solution). The influence of such parameters has been studied (Deitzel, Kleinmeyer, Harris, & Beck Tan, 2001; Tungprapa, Puangpam, et al., 2007). The electrospinning technique has been widely used, for fabricating fibrous structures based on biocompatible–biodegradable polymers and polymer–inorganic composite materials, especially for biomedical applications (Dalton, Klinkhammer, Salber, Klee, & Moller, 2006; Fujihara, Kotaki, & Ramakrishna, 2005; Marras, Kladi, Tsivintzelis, Zuburtikudis, & Panayiotou, 2008; Tserki, Philippou, & Panayiotou, 2006; Zhou, Green, & Joo, 2006).

Cellulose acetate (CA) is a well known derivative of cellulose and has been used in a broad field of applications such as adhesive, film base in photography or in separation processes (e.g. filtering, reverse osmosis) (Rodrigues Filho et al., 2008). Cellulose acetate is produced either by heterogeneous or homogeneous acetylation of cellulose (Rodrigues Filho et al., 2008; Wu, Jhang, He, Ren, & Guo, 2004). The homogeneous acetylation of cellulose and also the fabrication of porous and fibrous materials have been enabled by the use of ionic liquids as cellulose solvents (Tsioptsias & Panayiotou, 2008; Tsioptsias, Stefopoulos, Kokkinomalis, Papadopoulou, & Panayiotou, 2008; Viswanathan et al., 2006; Wu et al., 2004). In contrast to cellulose, cellulose acetate possesses a much less crystalline structure and thus exhibits better solubility in common organic solvents such as acetone. Porous structures based on CA have been developed (Fischer, Rigacci, Pirard, Berthon-Fabry, & Achard, 2006; Reverchon & Cardea, 2007). However, since CA is widely used as synthetic fiber, preparation of CA fibrous structures is more popular. CA fibrous structures have been produced via the electrospinning technique and the influence of different parameters on the fiber size and morphology (such as nature of solvent and applied voltage) has been extensively studied (Han, Youk, Min, Kang, & Park, 2008; Tungprapa, Puangpam, et al., 2007). Also encapsulation of drugs and other substances into CA nanofibers has been reported (Chen, Bromberg, Hatton, & Rutledge, 2008; Tungprapa, Jangchud, & Supaphol, 2007). Electrospun CA

* Corresponding author at: Department of Chemical Engineering, Aristotle University of Thessaloniki, University Campus, 54124 Thessaloniki, Greece.
Tel.: +30 2310 996223; fax: +30 2310 996232.
E-mail address: cpanayio@auth.gr (C. Panayiotou).
[1] Current address: Department of Chemical and Biochemical Engineering, Technical University of Denmark.

0144-8617/$ – see front matter © 2010 Elsevier Ltd. All rights reserved.
doi:10.1016/j.carbpol.2010.04.005

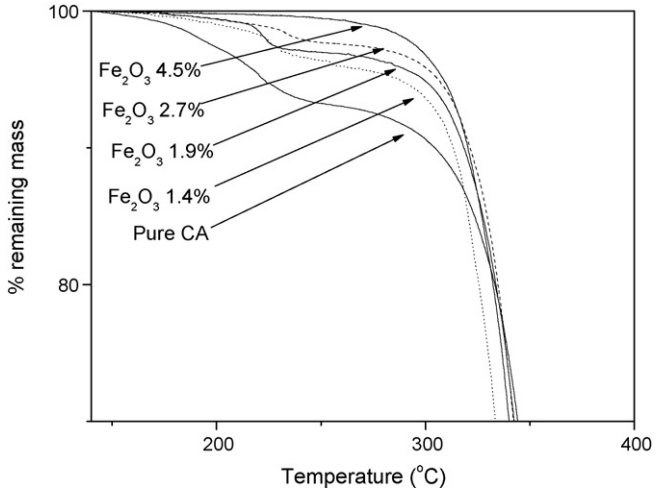

Fig. 1. TGA curves (for mass loss 0–30%) of cellulose acetate and cellulose acetate–iron oxide composite materials.

Table 1
Temperature of 3% loss mass and temperature of maximum decomposition rate of cellulose acetate and cellulose acetate–iron oxide composite materials.

% (w/w) Fe_2O_3 content in 20% (w/v) polymer solution	Temperature of 3% mass loss (°C)	Temperature of maximum decomposition rate (°C)
0% Fe_2O_3	205	358
1.4% Fe_2O_3	233	342
1.9% Fe_2O_3	246	345
2.7% Fe_2O_3	284	353
4.5% Fe_2O_3	299	351

membranes have been used in separation processes (Ma, Kotaki, & Ramakrishna, 2005; Zhang, Menkhaus, & Fong, 2008). CA–silver composite (Son, Youk, & Park, 2006) and CA–polymer blends (Chen, Wang, & Huang, 2007; Zhang & Hsieh, 2008) have been successfully electrospun. Other CA–polymer blends have been used as tissue engineering scaffolds (Entcheva et al., 2004; Salgado et al., 2002).

Iron oxides (Fe_3O_4 and Fe_2O_3) exhibit biocompatibility and magnetic properties and have gained attention, in the field of biomedical applications, for clinical diagnosis (imaging) and cell labeling, drug targeting, and enzyme immobilization (Heymer et al., 2008; Morales et al., 2008). Usually iron oxide nanoparticles are synthesized in situ in a polymer solution and a polymer–iron oxide composite is obtained. Although the in situ synthesis exhibits certain advantages (e.g. control of particle size), it can be applied mainly to water-soluble polymers. By this approach, a gelatin–iron oxide composite material has been developed and it was proposed as tissue engineering scaffold (Hu, Liu, Tsai, & Chen, 2007).

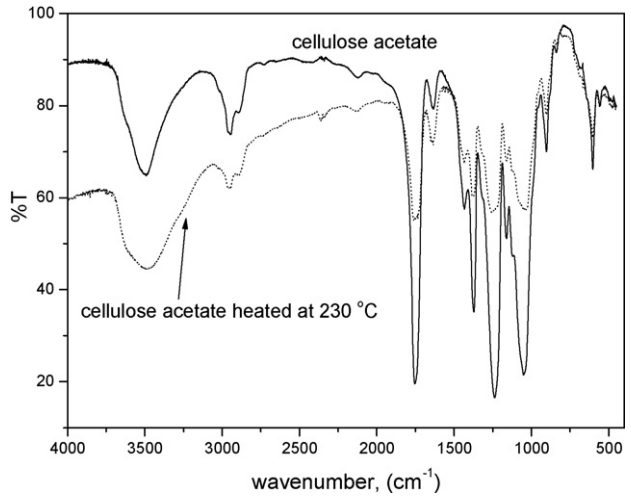

Fig. 2. FTIR spectra of cellulose acetate and cellulose acetate partially degraded (heated up to 230 °C).

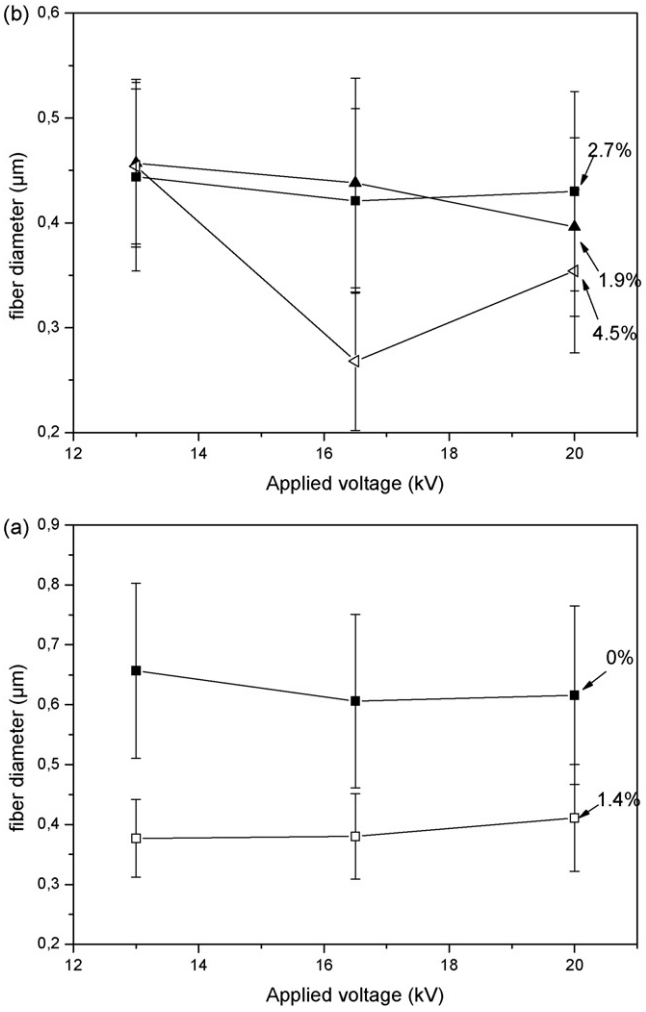

Fig. 3. Average fiber diameter of the produced samples as function of applied voltage and iron oxide content.

In this study, cellulose acetate–iron oxide composite materials with nanofibrous structure were developed via the electrospinning technique. The iron oxide nanoparticles were dispersed in the polymer solution at different concentrations. The influence of iron oxide concentration on the fiber size and morphology and on the thermal behavior of the materials was examined. The produced materials have potential use in separation processes and in biomedical applications (e.g. tissue engineering scaffolds).

2. Experimental

2.1. Materials and instruments

Cellulose acetate (Mn = 30,000, 39.8 wt% acetyl content) and iron(III) oxide (nanopowder, particle size <50 nm) were purchased from Sigma Aldrich. N,N-dimethylacetamide (purity > 98%) was purchased from Fluka. All other chemicals were purchased from Merck. All chemicals were used as received.

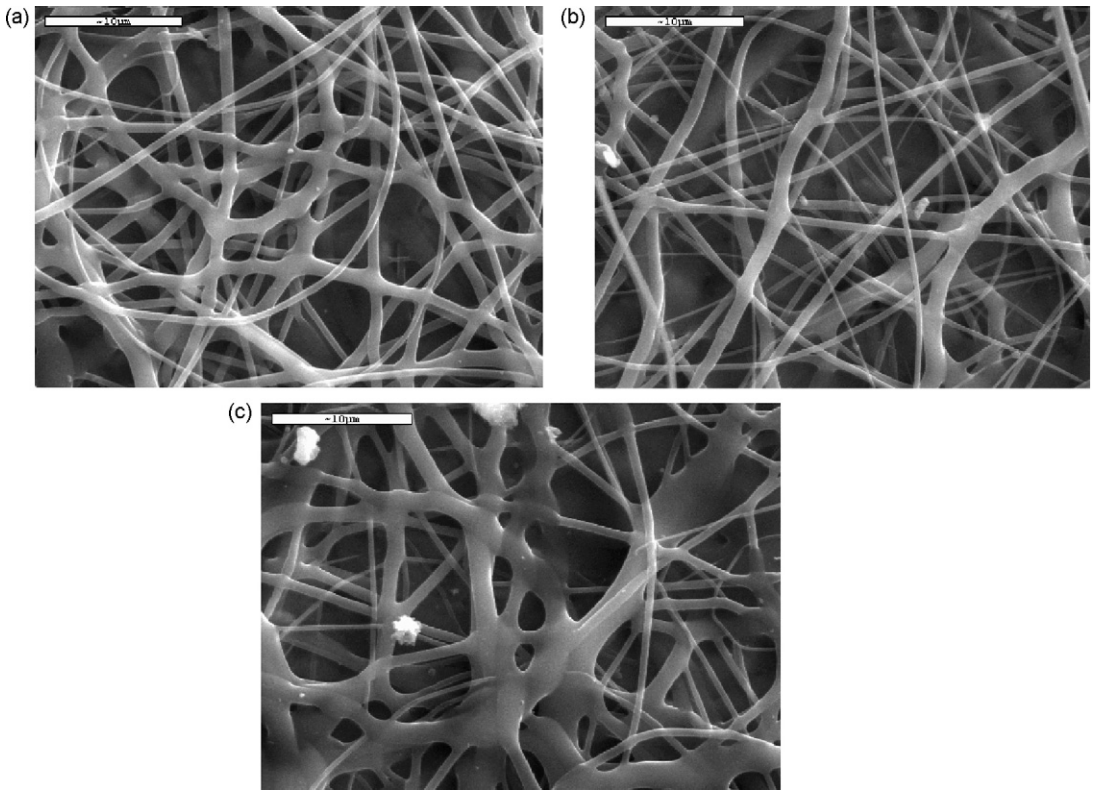

Fig. 4. SEM pictures of pure cellulose acetate samples for different applied voltages: (a) 13 kV; (b) 16.5 kV; (c) 20 kV.

The home-made electrospinning apparatus that was used is described in detail elsewhere (Marras et al., 2008; Tserki et al., 2006). Briefly, it consists of a cylindrical drum rotating along its axis, a high-voltage supplier (Spellman High Voltage DC SUPPLY, model RHR30P30) and a syringe pump (HARVARD APPARATUS, model 2274). The polymer solution was flowing through a needle of 1 mm inside diameter.

The morphology of the produced materials was examined with a Jeol (JSM-840A) scanning electron microscope (SEM). Average fiber diameter was calculated from the SEM pictures by the use of appropriate software. Calorimetric and thermogravimetric measurements were carried out with a Shimadzu differential scanning calorimeter (DSC-50) and a Shimadzu thermogravimetric analyzer (TGA-50) respectively. Also a conductive-meter (WTW, type LBR), a Cannon Fenske viscometer and an ultra sonicator (HEAT SYSTEMS-ULTRASONICS, INC., W-375) were used during the experiments. Infrared spectroscopic measurements were carried out with a Biorad FTS-175 spectrometer.

2.2. Solution and composite materials preparation

All solutions used in the experiments had concentration in cellulose acetate 20% (w/v). The solvent was mixture of acetone and N,N-dimethylacetamide (DMA) in 2/1 (acetone to DMA) volume proportion. Five solutions were prepared with only difference in the concentration of the dispersed particles of Fe_2O_3 (0%, 1.4%, 1.9%, 2.7%, 4.5% (w/v)).

The procedure for the solution preparation was as follows: cellulose acetate and Fe_2O_3 were accurately weighted in a Sartorius scale (±0.1 mg accuracy) at certain proportion in order to obtain the desired concentrations. Then, the weighted solids were placed in a glass and acetone was added in order to form a dilute dispersion. Dissolution of the polymer and dispersion of the Fe_2O_3 particles were rapidly achieved by application of ultrasound. During this procedure evaporation of acetone occurred. After complete dissolution and dispersion, the solutions were cast in Petri-dishes at room temperature in a fume hood. Operation of the fume hood ensured an unsaturated atmosphere, which results in a more intense solvent evaporation and this, in turn, results in a faster increase in the viscosity of the solution. As the viscosity of the solution increases sedimentation of the dispersed particles is prevented. After evaporation of the solvent at room temperature for at least 12 h, the films were further dried for another 12 h under vacuum at 60 °C. Then they were dissolved in the mixture of acetone and DMA in the desired concentrations. To avoid sedimentation of the particles, the dissolution of the films was carried out in a shaking bath at room temperature.

These solutions were used for the electrospinning experiments and for the viscosity and conductivity measurements. The conductivity measurements were carried out at room temperature (~27 °C) and the viscosity measurements at 24.96 ± 0.02 °C.

The dry films (pure cellulose acetate and cellulose acetate–Fe_2O_3 composite materials) besides the solutions preparation were also used for the DSC and TGA measurements. TGA was performed at air atmosphere, with a heating rate of 10 °C/min up to 100 °C, the temperature was held at 100 °C for 10 min, and then with a heating rate of 10 °C/min the temperature was increased up to 700 °C. The mass at 140 °C was set as the 100% mass. DSC measurements were performed using a heating rate of 5 °C/min under a constant nitrogen flow of 20 $cm^3\,min^{-1}$. The sample weight was kept at low levels (5 mg) in order to minimize any possible thermal lag during the scans. Two samples of cellulose acetate were examined with FTIR. One sample was from the above-mentioned dry cellulose acetate film. A small quantity of this sample was placed in the TGA and heated in air atmosphere with a heating rate of 10 °C/min up to 230 °C. Afterwards it was removed from the TGA and examined with FTIR. The FTIR measurements were performed with a resolution of 2 cm^{-1} and 16 scans. The samples were mixed with KBr and processed into pellets.

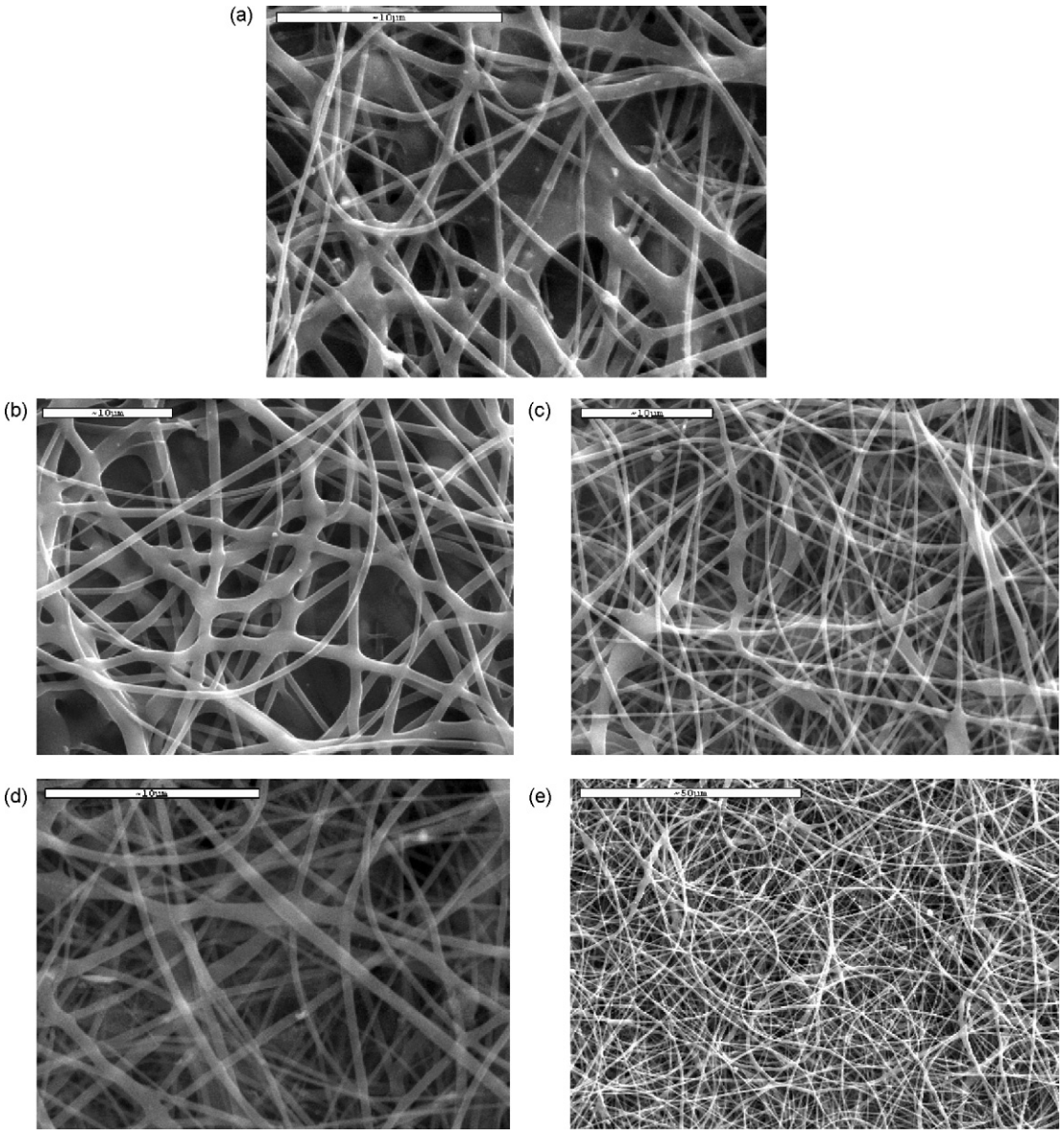

Fig. 5. Representative SEM pictures of the produced materials: (a) 0% and 13 kV; (b) 1.4% and 13 kV; (c) 1.9% and 13 kV; (d) 2.7% and 13 kV; (e) 4.5% and 20 kV.

2.3. Electrospinning experiments

The electrospinning of the solutions was carried out by keeping constant flow solution rate (0.38 ml/h), constant needle to target distance (5 cm) and by applying three different voltages (13, 16.5, 20 kV) between the target and the needle. The target was a rotating drum covered with aluminum foil. The samples were observed with SEM.

3. Results and discussion

3.1. Thermal behavior of the composite materials

In Fig. 1 the TGA curves are presented. In Table 1 the temperatures at which 3% mass loss occurs and the temperatures of maximum decomposition rate are presented. The temperature of maximum decomposition rate was estimated from the differential TGA curves (curves not shown).

The addition of iron oxide does not have any tremendous influence on the glass transition temperature of the material. For all materials, the glass transition temperature was $180 \pm 10\,^{\circ}C$. In contrast to this, the thermal stability of the materials is strongly influenced by the iron oxide content (Fig. 1 and Table 1). For example, by increasing the iron oxide content from 0% to 1.9%, in order to have 3% mass loss (or 97% remaining mass), the material must be heated to 205 and 246 °C (respectively for 0% and 1.9% iron oxide content). The composite materials start to degrade in higher temperatures, however the maximum decomposition rate occurs for all samples in the narrow temperature range between 340 and 360 °C. Also it is worth mentioning that all samples, at around 230 °C exhibit a sharp alteration in the slope of the mass loss curve. This sharp alteration becomes less intense by increasing the iron oxide content.

To examine which groups are responsible for this, a cellulose acetate sample was heated up to 230 °C and the FTIR spectra was compared with a thermally untreated cellulose acetate sample. The FTIR spectra are presented in Fig. 2. As can be seen there is a dramatic reduction in the intense of the peaks corresponding to the absorption at wavenumbers between 1000 and 1800 cm^{-1}. The band at $\sim$1750 cm^{-1} corresponds to the C=O stretching of ester groups (carbonyl groups) (Rodrigues Filho et al., 2008). The absorbance of C=O stretching at 1750 cm^{-1}, was compared to the

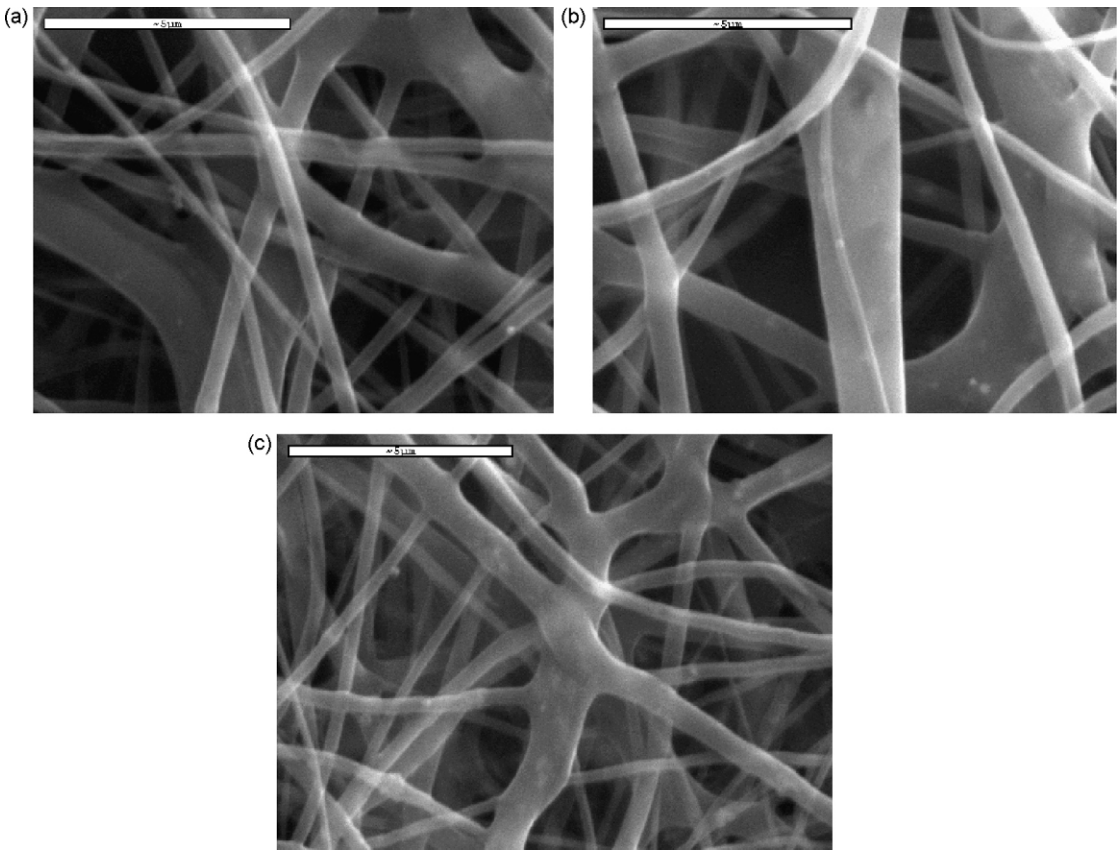

Fig. 6. Representative SEM pictures of the produced materials at higher magnifications (scale bar 5 μm): (a) 1.9% and 20 kV; (b) 2.7% and 20 kV (c) 4.5% and 13 kV.

absorbance of OH stretching at 3480 cm^{-1}. The absorbance ratio A_{3480}/A_{1750} was found to be 0.2 (for the cellulose acetate sample) and 0.98 for (the sample heated to 230 °C). This increase in the ratio indicates a considerable decrease in the ester groups compared to hydroxyl groups. Similar increases were found for other band ratios such as A_{3480}/A_{1050} (C–O–C stretching) and A_{3480}/A_{1255} (C–O).

3.2. Fibrous structures of cellulose acetate–iron oxide composites

In Fig. 3 the average fiber diameter (average value ± average deviation from the average value) of all the produced samples is presented, and the influence of applied voltage and iron oxide concentration on the fiber size can be seen. Usually the increase of applied voltage leads to decrease in average fiber size (Zhou et al., 2006). However, a different behavior was observed in our case. As can be seen in Fig. 3a and b and in Fig. 4 (SEM pictures of cellulose acetate fibrous structures for three different voltages), by increasing the applied voltage the structure becomes less uniform (almost same average value but a small increase in deviation). Similar are the conclusions for the composite materials regarding the influence of voltage. For the explanation of this, it must be taken into account that the solvent mixture that was used had a quite high boiling point (due to the addition of DMA) and in contrast to common volatile organic solvents (e.g. dichloromethane, acetone, chloroform) the solvent used in the experiments was not so volatile. By increasing voltage the instability of the jet becomes more intense, and thus, the fibers are formed in a more random and rapid way. The more random production of fibers may result, to some extent, less uniform structures. Also, less time is available for solvent evaporation as the production of the fibers becomes more rapid. Subsequently, residual solvent remains in the fibers when they reach the target. This leads to coalescence of neighboring fibers and thus the produced structure is less uniform.

Rather peculiar were the results considering the influence of iron oxide concentration on the fiber size. By adding only 1.4% of iron oxide, a dramatic decrease in the average fiber diameter is observed (independently from the applied voltage), as can be seen in Fig. 3a. However, further increase of the iron oxide content does not seem to have any major influence on the fiber size (Fig. 3b). Usually, by increasing the concentration of the solution, the fiber size is also increased, due to increase in the viscosity (Deitzel et al., 2001). Also by increasing the conductivity of the solution the fiber size decreases (Marras et al., 2008; Zong et al., 2002).

The electric conductivity and viscosity measurements of the solutions are presented in Table 2. As can be seen, by increasing the iron oxide content the conductivity also increases in all cases. The viscosity however, decreases (compared to the pure polymer solution) when iron oxide is added in 1.4% but increases for all other iron oxide concentrations. It must be taken into account that the addition of the nanoparticles into the polymer solution has a double effect. Firstly, it is reasonable to expect increased viscosity due to the increase of the total dispersion concentration. However, the solid nanoparticles hinder polymer chain interactions by increasing their distance. The second phenomenon prevails in the 1.4% iron oxide dispersion, while with further increase of iron oxide content, the first phenomenon becomes dominant and the expected increase of the viscosity is observed. It should be mentioned here, that unexpected decrease in viscosity of polymer blend, due to nanoscale effects, has been reported in the literature (Mackay et al., 2003).

Thus when adding 1.4% of iron oxide, both the increase in the conductivity and the decrease in the viscosity tend to decrease the fiber size. This is the explanation for the dramatic decrease in the

Table 2
Viscosity and conductivity of the solutions used in electrospinning experiments.

% (w/v) Fe_2O_3 content in 20% (w/v) polymer solution	Viscosity at 24.96 ± 0.02 °C (cSt)	Conductivity at 27 °C (S/cm)
0% Fe_2O_3	781.2	5×10^{-6}
1.4% Fe_2O_3	718.6	8.6×10^{-6}
1.9% Fe_2O_3	789.8	1.2×10^{-5}
2.7% Fe_2O_3	850.3	1.4×10^{-5}
4.5% Fe_2O_3	858.9	1.6×10^{-5}

fiber size in the 1.4% composite material. By increasing even more the iron oxide content, the conductivity increases (tendency for smaller fiber size) but also the viscosity increases (tendency for larger fibers). These two effects seem to cancel out each other, and no tremendous influence of the iron oxide content on the fiber size can be seen.

Representative SEM pictures of the composite materials are presented in Figs. 5 and 6. In Fig. 6 high magnification (10,000× or 9000×) images can be seen. In the 4.5% composite some iron oxide aggregates can be seen upon the fibers. In the composite of 2.7%, iron oxide aggregates are hardly visible, while in the composites of lower iron oxide content, no aggregates can be seen. These are evidence for good dispersion of the particles into the polymer matrix and are in agreement with the TGA results.

Finally it is worth mentioning that all of the composite materials could be magnetized. Thus, they could possibly be used in advanced separation processes induced by external magnetic field (separation due to pore structure and due to magnetism), for controlled drug delivery or in more common applications of polymer–iron oxide composites such as sound recording media (magnetic tapes).

4. Conclusions

Cellulose acetate–iron oxide composite nanofibrous materials were successfully prepared via the electrospinning technique. The composite materials exhibit enhanced thermal stability compared to pure cellulose acetate. The addition of iron oxide in 1.4% concentration causes a decrease in the viscosity and increase in the conductivity of the solution, which lead to a considerable decrease in the fibers diameter. Further addition of iron oxide does not have any tremendous influence on the fibers size, due to the competitive effects of viscosity and conductivity increase. At higher values of applied voltages, less uniform structures are produced, due to incomplete solvent evaporation (fiber coalescence occurs). The produced materials could be used in biomedical applications (e.g. tissue engineering scaffolds) or in high temperature separation processes (e.g. filters).

References

Chen, L., Bromberg, L., Hatton, T. A., & Rutledge, G. C. (2008). Electrospun cellulose acetate fibers containing chlohexidine as a bactericide. *Polymer*, *49*, 1266–1275.

Chen, C., Wang, L., & Huang, Y. (2007). Electrospinning of thermo-regulating ultrafine fibers based on polyethylene glycol/cellulose acetate composite. *Polymer*, *48*, 5202–5207.

Dalton, P. D., Klinkhammer, K., Salber, J., Klee, D., & Moller, M. (2006). Direct in vitro electrospinning with polymer melts. *Biomacromolecules, 7*, 686–690.

Deitzel, J. M., Kleinmeyer, J., Harris, D., & Beck Tan, N. C. (2001). The effect of processing variables on the morphology of electrospun nanofibers and textiles. *Polymer*, *42*, 261–272.

Entcheva, E., Bien, H., Yin, L., Chung, C. Y., Farrell, M., & Kostov, Y. (2004). Functional cardiac cell constructs on cellulose-based scaffolding. *Biomaterials*, *25*, 5753–5762.

Fischer, F., Rigacci, A., Pirard, R., Berthon-Fabry, S., & Achard, P. (2006). Cellulose-based aerogels. *Polymer*, *47*, 7636–7645.

Fujihara, K., Kotaki, M., & Ramakrishna, S. (2005). Guided bone regeneration membrane made of polycaprolactone/calcium carbonate composite nanofibers. *Biomaterials*, *26*, 4139–4147.

Han, S. O., Youk, J. H., Min, K. D., Kang, Y. O., & Park, W. H. (2008). Electrospinning of cellulose acetate nanofibers using a mixed solvent of acetic acid/water: Effects of solvent composition on the fiber diameter. *Materials Letters*, *62*, 759–762.

Heymer, A., Haddad, D., Weber, M., Gbureck, U., Jakob, P. M., Eulert, J., & Noth, U. (2008). Iron oxide labeling of human mesenchymal stem cells in collagen hydrogels for articular cartilage repair. *Biomaterials*, *29*, 1473–1483.

Hu, S. H., Liu, T. Y., Tsai, C. H., & Chen, S. Y. (2007). Preparation and characterization of magnetic ferroscaffolds for tissue engineering. *Journal of Magnetism and Magnetic Materials*, *310*, 2871–2873.

Ma, Z., Kotaki, M., & Ramakrishna, S. (2005). Electrospun cellulose nanofibers as affinity membrane. *Journal of Membrane Science*, *265*, 115–123.

Mackay, M. E., Dao, T. T., Tuteja, A., Ho, D. L., Van Horn, B., Kim, H. C., & Hawker, C. J. (2003). Nanoscale effects leading to non-Einstein-like decrease in viscosity. *Nature Materials*, *2*, 762–766.

Marras, S. I., Kladi, K. P., Tsivintzelis, I., Zuburtikudis, I., & Panayiotou, C. (2008). Biodegradable polymer nanocomposites: The role of nanoclays on the thermomechanical characteristics and the electrospun fibrous structure. *Acta Biomaterialia*, *4*, 756–765.

Morales, M. A., Finotelli, P. V., Coaquira, J. A. H., Rocha-Leao, M. H. M., Diaz-Aguila, C., Baggio-Saitovitch, E. M., & Rossi, A. M. (2008). In situ synthesis and magnetic studies of iron oxide nanoparticles in calcium–alginate matrix for biomedical applications. *Materials Science and Engineering C*, *28*, 253–257.

Reverchon, E., & Cardea, S. (2007). Production of controlled polymeric foams by supercritical CO_2. *The Journal of Supercritical Fluids*, *40*, 144–152.

Rodrigues Filho, G., Monteiro, D. S., da Silva Meireles, C., Assuncao, R. M. N., Cerqueira, D. A., Barud, H. S., Ribeiro, S. J. L., & Messadeq, Y. (2008). Synthesis and characterization of cellulose acetate produced from recycled newspaper. *Carbohydrate Polymers*, *73*, 74–82.

Salgado, A. J., Gomes, M. E., Chou, A., Coutinho, O. P., Reis, R. L., & Hutmacher, D. W. (2002). Preliminary study on the adhesion and proliferation of human osteoblasts on starch-based scaffolds. *Materials Science and Engineering C*, *20*, 27–33.

Son, W. K., Youk, J. H., & Park, W. H. (2006). Antimicrobial cellulose acetate nanofibers containing silver nanoparticles. *Carbohydrate Polymers*, *65*, 430–434.

Tserki, V., Philippou, J., & Panayiotou, C. (2006). Preparation and characterization of electrospun poly(butylene succinate–co–butylene adipate) nanofibrous nonwoven mats. In *Proceedings of the I MECH E Part N Journal of Nanoengineering and Nanosystems, Vol. 220* (pp. 71–79).

Tsioptsias, C., & Panayiotou, C. (2008). Preparation of cellulose–nanohydroxyapatite composite scaffolds from ionic liquid solutions. *Carbohydrate Polymers*, *74*, 99–105.

Tsioptsias, C., Stefopoulos, A., Kokkinomalis, I., Papadopoulou, L., & Panayiotou, C. (2008). Development of micro- and nano-porous composite materials by processing cellulose with ionic liquids and supercritical CO_2. *Green Chemistry*, *10*, 965–971.

Tungprapa, S., Jangchud, I., & Supaphol, P. (2007). Release characteristics of four model drugs from drug-loaded electrospun cellulose acetate fiber mats. *Polymer*, *48*, 5030–5041.

Tungprapa, S., Puangpam, T., Weerasombut, M., Jangchud, I., Fakum, P., Semongkhol, S., Meechaisue, C., & Supaphol, P. (2007). Electrospun cellulose acetate fibers: Effect of solvent system on morphology and fiber diameter. *Cellulose*, *14*, 563–575.

Viswanathan, G., Murugesan, S., Pushparaj, V., Nalamasu, O., Ajayan, P. M., & Linhardt, R. J. (2006). Preparation of biopolymer fibers by electrospinning from room temperature ionic liquids. *Biomacromolecules*, *7*, 415–418.

Wu, J., Jhang, H., He, J., Ren, Q., & Guo, M. (2004). Homogeneous acetylation of cellulose in a new ionic liquid. *Biomacromolecules*, *5*, 266–268.

Zhang, L., & Hsieh, Y. L. (2008). Ultra-fine cellulose acetate/poly(ethylene oxide) biocomponent fibers. *Carbohydrate Polymers*, *71*, 196–207.

Zhang, L., Menkhaus, T. J., & Fong, H. (2008). Fabrication and bioseparation studies of adsorptive membranes/felts made from electrospun cellulose acetate nanofibers. *Journal of Membrane Science*, *319*, 176–184.

Zhou, H., Green, T. B., & Joo, Y. L. (2006). The thermal effects on electrospinning of polylactic acid melts. *Polymer*, *47*, 7497–7505.

Zong, X., Kim, K., Fang, D., Ran, S., Hsiao, S. B., & Chu, B. (2002). Structure and process relationship of electrospun bioabsorbable nanofiber membranes. *Polymer*, *43*, 4403–4412.